Computational Design of a Light-Driven Molecular Motor

Nicolae M. Albu, Edward Bergin, and David J. Yaron*

Department of Chemistry, Carnegie Mellon University, 4400 Fifth Avenue, Pittsburgh, Pennsylvania 15213

Received: December 31, 2008; Revised Manuscript Received: May 6, 2009

Light-driven molecular motors may be useful for nanotechnology applications. The possibility of building such a motor based on the tolane framework is explored here. In the ground electronic state of tolane, the barrier to internal rotation is comparable to room temperature thermal energies, k_BT. The barrier increases substantially in the excited state, causing the molecule to planarize after absorption of a photon. This tendency to planarize may be converted into unidirectional rotational motion by placing chiral substituents on the phenyl rings. A potential advantage of this class of motors is that they may undergo rapid, nanosecond scale rotation. Computational design of appropriate substituents was done using semiempirical quantum chemical methods, SAM1 for the ground electronic state coupled to INDO for the excitation energy. The torsional surfaces of the best candidate were then generated using ab initio DFT methods, which confirm that the molecule should undergo unidirectional rotation upon photoexcitation. The results provide a proof of principle for this class of motors; however, two aspects of the final candidate are nonideal. First, although the design goal was to use steric interactions between substituents to induce the rotation, decomposition of the interaction energy suggests attractive interactions play a role. Solvent interactions may interfere with these attractive interactions. Second, TDDFT calculations suggest that interactions between excited states lower the rotational driving force in the excited state.

1. Introduction

A potentially interesting building block for nanotechnology is the molecular motor.[1–16] Attempts to fabricate mechanical devices on the molecular level have yielded analogues of rotors,[17] gears,[18–20] brakes,[21] switches,[22] shuttles,[23,24] turnstiles,[25] and ratchets.[26] The main challenge in building molecular motors is attaining efficient and controlled conversion of chemical energy or photons into unidirectional rotary motion. A common current approach to the design of light-driven motors relies on photoinduced isomerizations coupled with thermalization steps.[3,7] The thermalization step is typically the rate-limiting step that establishes the rotation time. Here, we consider a different approach to the design of light-driven molecular motors. This new approach exploits the tendency of certain classes of conjugated molecules to planarize upon photoexcitation.

The base framework used here for our molecular motor design is tolane, which has two phenyl rings linked by a C−C triple bond as shown in Figure 1. The barrier to torsional rotation in the ground electronic state is about 0.57 kcal/mol.[27,28] This is roughly equivalent to k_BT at room temperature, and so many torsional angles are populated at room temperature. Electronic absorption and emission spectra on oligomers with three to nine phenyl rings can be fit with a simple exciton model in which an excitation hops coherently between sites.[29,30] The sites correspond to each of the phenyl rings, and the coupling between sites is given by $\beta\cos(\theta)$, where θ is the dihedral angle between adjacent phenyl rings. Within this exciton model, the excitation energy of tolane is given by the lowest eigenvalue of the following Hamiltonian matrix:

$$\hat{H} = \begin{pmatrix} \alpha & \beta\cos(\theta) \\ \beta\cos(\theta) & \alpha \end{pmatrix} \quad (1)$$

where α is the energy of the exciton on a single site. Fits of the oligomer spectra yield a value of 4.35 eV for α and −0.75 eV for β.

The excitation energy from eq 1 is to be added to the ground-state energy surface, as shown in Figure 2. Unlike the ground state, the torsional barrier in the excited state is large compared to k_BT, so the molecule planarizes following optical excitation; i.e., the wide distribution of torsional angles present in the ground state narrows after excitation to the excited state.

The planarization of tolane in the excited state corresponds to torsional motion that is driven by absorption of the photon.

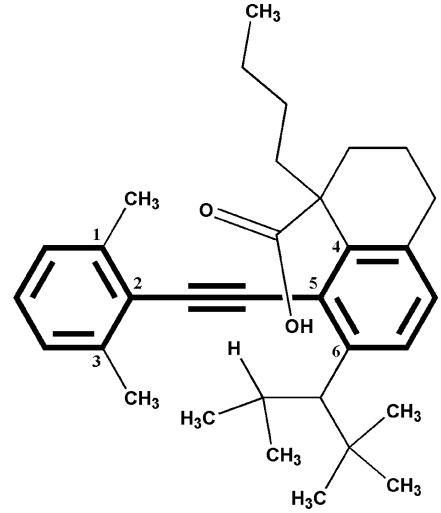

Figure 1. Best candidate motor molecule. The tolane framework is shown in bold along with the atom numbering scheme.

* To whom correspondence should be addressed. E-mail: yaron@cmu.edu. Phone: (412) 268-1351. Fax: (412) 268-1061.

10.1021/jp811521s CCC: $40.75
Published on Web 06/02/2009

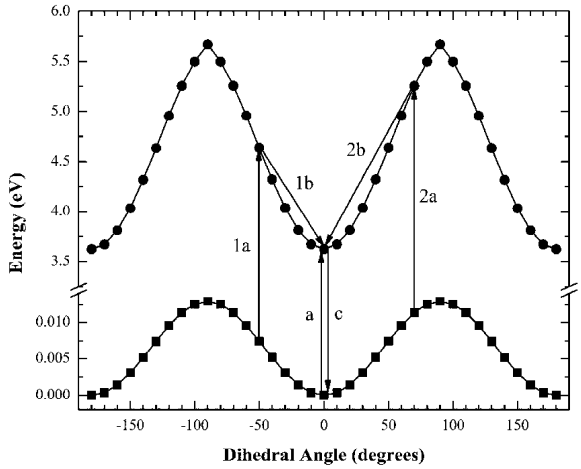

Figure 2. Idealized representation of the ground-state energy surface (■) and excited-state energy surface (●) as a function of the dihedral angle between the phenyl rings in tolane. The arrows illustrate optical excitation followed by torsional relaxation to the closest planar minimum.

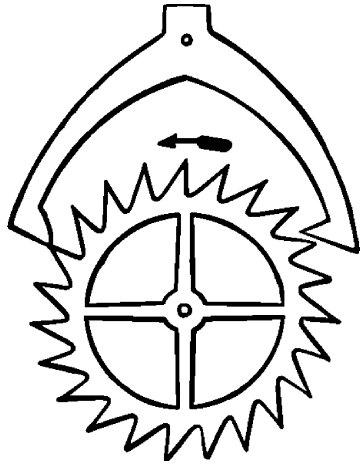

Figure 3. Clockwork: gear with escapement mechanism.

The goal here is to convert this nondirectional torsional motion into unidirectional rotational motion. A mechanical analogy can be drawn to the self-winding watch illustrated in Figure 3. The escapement mechanism converts random vibrations into unidirectional motion which winds the spring of the watch. For the molecular motor, the photoexcitation of the molecule is analogous to the random vibrations of the watch. The analogue to the escapement mechanism will be chemical substituents added to the tolane framework. Chiral substituents can break the left/right symmetry and preferentially favor rotation in one direction.

Given the vastly different torsional barriers in the ground and excited states, it is possible to add substituents whose interactions are sufficiently large that they dominate the ground-state surface while having little impact on the excited-state surface. Since the torsional barrier arises primarily from the π conjugation in the tolane core, steric effects between substituents attached to this core should be well modeled by adding a steric potential to both the ground- and excited-state surfaces. Figure 4 shows the result of adding ideal substituent effects to the surfaces of Figure 2. The results highlight that substituent effects can fundamentally change the nature of the ground-state surface while having little effect on the excited-state surface. Our design goal is to identify substituents that will induce a potential of this type.

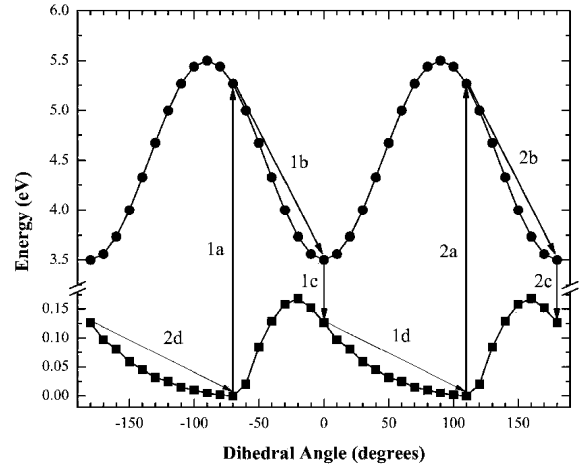

Figure 4. Steric effects change the ground-state surface (■) much more strongly than the excited-state surface (●) and promote unidirectional rotation motion. The arrows show the effects of optical excitation.

We next compare the torsional motion resulting from the idealized potentials of bare tolane (Figure 2) and substituted tolane (Figure 4). In Figure 2 both the ground- and excited-state minima are at 0°. Optical excitation from the ground-state minimum is then to the excited-state minimum at 0° (arrow a), and no torsional relaxation results. Since the ground-state barrier of bare tolane is comparable to k_BT, many torsional angles are populated at room temperature. Arrows 1a−1b and 2a−2b illustrate that optical excitation from an angle that differs from zero will be followed by torsional relaxation to the closest planar minimum.

Chiral substitution of tolane is meant to convert this nondirectional torsional relaxation into unidirectional torsional motion. In Figure 4, substituent effects have increased the torsional barrier in the ground state such that the population is primarily at the minimum near −70°. Vertical excitation (arrow 1a) will lead to a position on the excited-state surface that relaxes (arrow 1b) in a clockwise (CW) direction to the excited-state minimum at 0°. Assuming relaxation back onto the ground-state surface occurs with little change in torsional angle (arrow 1c), the molecule reaches a point on the ground-state surface that again relaxes (arrow 1d) in a clockwise direction to the minimum at +110°. This +110° minimum is equivalent to that at −70°, so another cycle follows the path 2a−2b−2c−2d to return to the original minimum at −70°, and the rotational cycle then repeats.

There are two features of the torsional surfaces in Figure 4 that promote unidirectional rotation: (1) Vertical excitation from the ground-state minimum is to a point on the excited-state surface that relaxes preferentially in a clockwise direction. (2) The minimum of the excited-state surface drops to a point on the ground-state surface that relaxes preferentially in a clockwise direction.

A general strategy for achieving substituent effects similar to those of Figure 4 is shown in Figure 5. One of the phenyl rings is a rotor with two equivalent substituents symbolized by blue spheres. The other phenyl ring has chiral substituents that interact sterically with the rotor, functioning as a stator that promotes unidirectional motion.

The arrows labeled 1a−1d follow a half-rotation of the rotor, with one of the blue spheres labeled with a pink dot to aid in visualizing the 180° rotation. In the relaxed ground state, the rotor is near 90° to minimize the steric interaction with the stator. In addition, the interaction with the red sphere dominates the steric interactions near 90° and is sufficient to push the rotor past 90° in

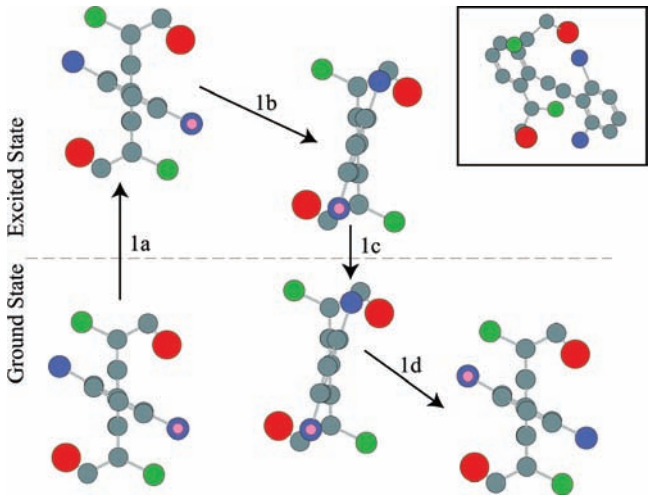

Figure 5. Schematic representation of the molecular motor, in which chiral substituents are used to impart unidirectional motion. Arrow 1a shows optical excitation, which leads to an increase in the torsional barrier. Arrow 1b shows how the rotor relaxes CW toward the nearest planar structure, past the green group. Arrow 1c shows the return to the ground state. Arrow 1d shows how the rotor relaxes in a CW direction past the red group.

the clockwise direction. Following vertical excitation (arrow 1a), the torsional potential of the tolane framework dominates over steric interactions and the rotor planarizes by rotating to the closest planar configuration, which is in the clockwise direction (arrow 1b). The red group of the stator thereby imparts feature 1 to our potential surfaces, causing excitation to be to a point on the excited-state surface that relaxes in a clockwise direction. The green sphere dominates the steric effects when the rotor is near the planar configuration. The red sphere is sufficiently far away at this point that when the molecule drops onto the ground-state surface (arrow 1c), rotation past the red sphere is more favorable than rotation past the green sphere. This leads to clockwise rotation (arrow 1d). A key factor here is the presence of two sets of steric interactions. One set is active near the planar structure and is shown here as a green sphere that is β to the phenyl ring. The other set is active near 90° and is shown here as a red sphere that is γ to the phenyl ring.

Hoki and co-workers also used chiral substitution on a conjugated framework to develop a molecular motor.[31] However, in their case, the motor is driven through femtosecond pump−dump laser pulses. A molecule, which is nonplanar in the ground electronic state, is first pumped to the Franck−Condon region of the excited-state surface. As the molecule relaxes toward the planar minimum of the excited state, it builds up torsional momentum. A dump laser pulse is then used to drop the molecule to the ground state, retaining sufficient torsional momentum that the molecule undergoes rotation on the ground-state surface. Rotation relies on an appropriate delay between the pump and dump pulses, since the molecule will not undergo a complete rotation if allowed to relax in the excited state. The goal here is to design a molecule that will rotate under continuous wave excitation. Our assumption is that the molecule will relax to the minimum of the excited-state surface following excitation, which is reasonable given that rotational relaxation typically occurs in tens of picoseconds.[32,33]

The above discussion is based on the simplified excitation energy of eq 1. In unsubstituted tolane, excited-state relaxation involves bending about the central triple bond into a *trans* configuration, as would be expected if the hybridization in the bridge took on sp^2 character.[27,34] For the motor of Figure 1, the strong steric interaction between the substituents likely prevents such bending from occurring. An additional complicating feature is curve crossings with higher excited electronic states. In longer oligomers, from which the parameters of eq 1 were derived, extended conjugation lowers the excitation energy such that these curve crossings are suppressed. We will see below that such curve crossings limit the available driving force for the motor.

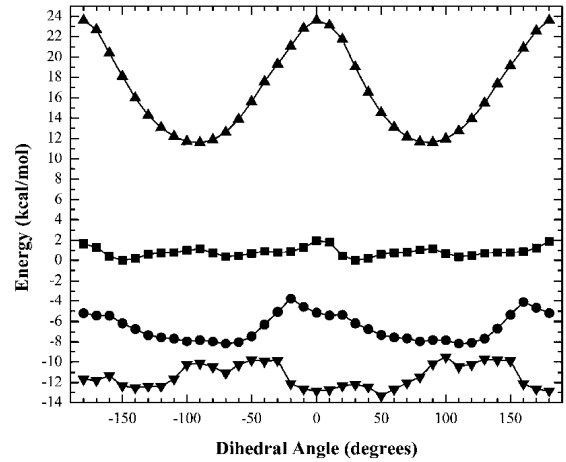

Figure 6. Ground-state energy of the best candidate motor (Figure 1) for PM3 (▼), SAM1 (●), AM1 (■), and MNDO (▲). Hamiltonians as a function of the dihedral angle C1−C2−C5−C6 between the phenyl rings. The surfaces are shifted in energy for better visualization.

Section 2 discusses the computational methods used to compute the ground- and excited-state torsional surfaces. Section 3 discusses the design strategy and presents our current best candidate for a molecular motor. More advanced methods for computing the ground-state energy and excitation energy are applied to the best candidate molecule in section 4. For a better understanding of the nature of the unidirectional rotation, section 5 discusses the decomposition of the interaction energies present in the best candidate. This is followed by a brief summary in section 6.

2. Methods

The rotational properties of the molecule are related to the torsional potential energy surfaces shown schematically in Figure 4. These are generated by a hybrid scheme that uses different methods for the ground-state and excitation energies:

$$\Delta E_{\text{excited state}} = \Delta E_{\text{ground state}} + \Delta E_{\text{excitation}} \qquad (2)$$

The SAM1 semiempirical method was used to compute the ground-state energy for initial screening of motor candidates. A comparison of results from the AM1, SAM1, MNDO, and PM3 Hamiltonians obtained with Semichem Ampac 8[35] for our best motor candidate (Figure 1) is shown in Figure 6. The surface is generated by constraining the dihedral angle C1−C2−C5−C6 in Figure 1. The results vary considerably with the method; however, the SAM1 surface is in good agreement with ab initio calculations (section 5) and so is the method used for our screening process. (Generating the torsional surface for a single candidate takes 6 h with SAM1, as compared to over two months for ab initio theory).

To allow screening of a large number of candidate molecules, the excitation energy, $\Delta E_{\text{excitation}}$ of eq 2, was initially obtained from the lowest eigenvalue of eq 1:[29,30]

$$\Delta E_{\text{excitation}} = 4.35 - 0.75|\cos(\theta)| \text{ (eV)} \quad (3)$$

where θ is the dihedral angle C1−C2−C5−C6 of Figure 1. More advanced models of the excitation energy are considered in section 5.

3. Design of the Motor

The goal of the design was to place groups on the rotor and stator that will induce the two key features identified in section 1 as needed for a light-driven molecular motor. Given the large space of possible groups, screening of motor candidates was done using the semiempirical methods discussed in section 2. The torsional surfaces for the best candidate of Figure 1, obtained using these screening methods, are shown as the filled squares and open circles of Figure 7. These surfaces show the desired ground- and excited-state surface features: (1) Excitation from the ground-state minimum is to a position on the excited-state surface with a strong driving force in the CW direction (toward larger angles in Figure 7). At room temperature, more than 87% of the ground-state population is in the minimum at −70°/110°. (2) Relaxation from the excited-state minimum is to a point on the ground-state surface with a strong driving force in the CW direction.

A large number of candidate molecules were explored, and some general design features emerged. For the groups on the rotor, the blue groups of Figure 5, both methyl and halides were tried and methyl was found to be best for obtaining interactions of the desired magnitude with groups on the stator. The general goal is to put groups on the stator that will play the role of the green and red groups of Figure 5 by breaking the CW/counterclockwise (CCW) symmetry of the rotor motion. Experimentation led to some general insights into how to best design the stator. First is the need to keep the groups placed on the stator pointing toward the rotor. The cyclohexane ring on the upper portion of the stator in Figure 1 provides a convenient means to force the stator groups to point toward the rotor. The hydrocarbons on the lower portion of the stator are sufficiently bulky that they are highly constrained and so have a predictable interaction with the rotor. Second is the use of different substituent groups on the upper versus lower portion of the stator. When identical groups are used on the upper and lower portions, it is difficult to find groups that have moderate interaction energy with the rotor. This is due to the strong, exponential dependence of steric interactions on distance, such that the available chemical substituents lead to interactions with the rotor that are either too large or too small. By using different groups on the upper and lower portions of the stator, the triple bond linking the phenyl rings can bend slightly as the rotor turns, effectively allowing the groups on the rotor and stator to slide over one another and maintain reasonable interaction energy throughout the rotor motion. Despite these general guidelines, identification of a molecule with the desired features was challenging. Changing the chemical substituents in a manner that appeared reasonable often led to unforeseen and undesirable consequences. The molecule of Figure 1 is the best candidate we could identify using the semiempirical methods described above.

4. Higher Level Calculations on the Best Candidate

A. Ground-State Torsional Surfaces. The above molecular design used the SAM1 Hamiltonian to generate the torsional surfaces. To test our choice of SAM1 Hamiltonian, we also generated the ground-state torsional surface at the Hartree−Fock level with the 3-21G basis set, using the GAUSSIAN03 quantum chemistry program.[36] For each dihedral angle two calculations were performed: one with only one dihedral angle fixed (C1−C2−C5−C6 in Figure 1) and one with all four dihedral angles between the rings fixed (C1−C2−C5−C6, C1−C2−C5−C4, C3−C2−C5−C6, and C3−C2−C5−C4 in Figure 1). The results of these calculations are shown in Figure 8 along with the SAM1 optimization results.

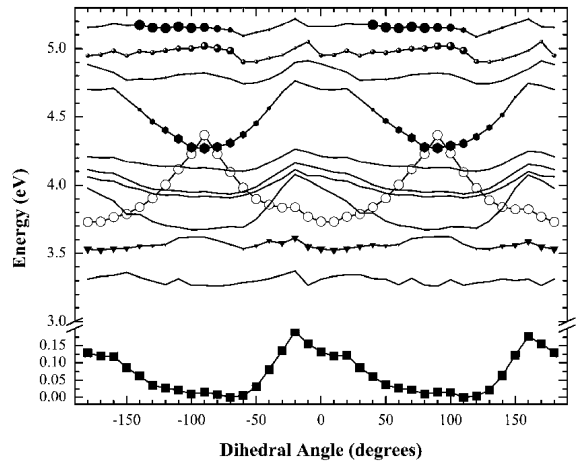

Figure 7. Computed torsional potentials for the motor shown in Figure 1. The design of the molecule used SAM1 for the ground-state energy (■) and eq 3 for the excitation energy (○). The remaining lines show vertical excitation energies from INDO theory, with symbol sizes proportional to the optical intensity from the ground state. The dihedral angle is defined such that the methyl on the rotor is closer to the carboxylic acid group at 110° than it is at 90°.

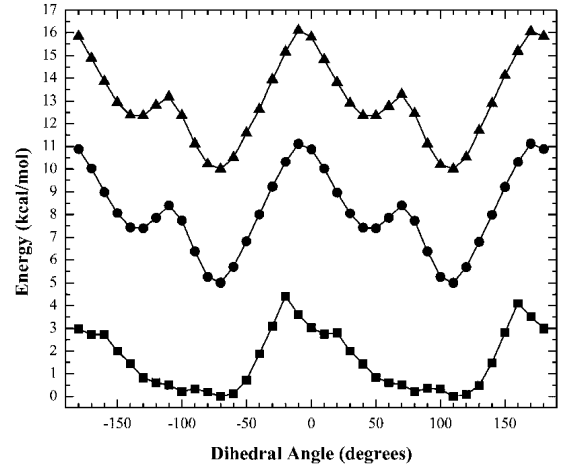

Figure 8. Ground states of our best candidate as a function of the dihedral angle with SAM1 ground-state geometry optimization (■, C1−C2−C5−C6) and ab initio calculation for one frozen dihedral angle (▲, C1−C2−C5−C6) and for all four frozen dihedral angles (●, C1−C2−C5−C6, C1−C2−C5−C4, C3−C2−C5−C6, and C3−C2−C5−C4). The surfaces are shifted in energy for better visualization.

The ab initio and SAM1 surfaces are in agreement regarding the key features needed for unidirectional motion. The first feature is that the global minimum of the ground state be at angles greater than 90°. SAM1 and ab initio methods agree on the location of the global minimum. SAM1 finds a local minimum somewhat below 90° with energy only slightly above the global minimum. Ab initio theory also finds such a local minimum, but with a considerably higher energy such that the population of this local minimum is negligible, provided the system is thermally equilibrated. The second feature is that the molecule continues to rotate in a clockwise direction after

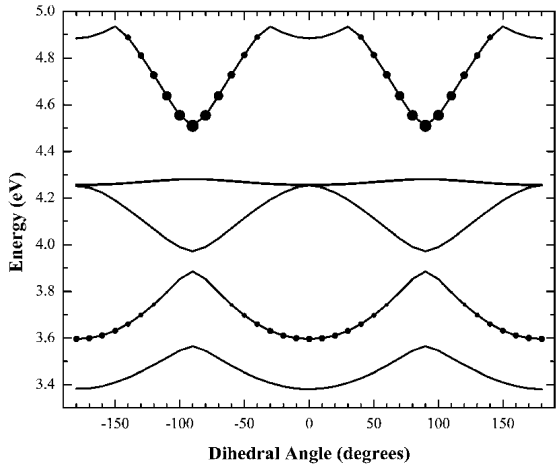

Figure 9. Excited states of tolane as a function of the dihedral angle (C1−C2−C5−C6 of Figure 1) calculated by adding the vertical INDO excitation energy to the SAM1 ground-state energy. The size of the symbols is proportional to the optical intensity from the ground electronic state.

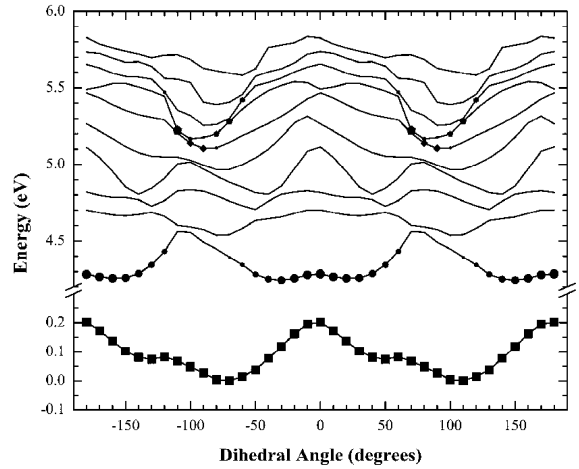

Figure 10. Ab initio calculations for the best candidate molecule of Figure 1. Geometries are from optimization of the ground electronic state using HF with a 3-21G basis set. Single-point calculations with the B3LYP functional and 6-31G(d,p) basis set were then performed for the DFT ground state (■) and first 10 TDDFT excited states (●, ◆, ..., with the symbol size proportional to the optical intensity from the ground state).

relaxation from the excited to ground state. Since the excited-state minimum is near 0°, this requires that the maximum in the ground-state surface be below 0°. This feature is also present in both the SAM1 and ab initio surfaces. The only feature in the ab initio surface that could potentially hinder the functionality of the rotor is the local minimum at 50° with a 1.02 kcal/mol barrier separating it from the global minimum. Since this barrier is only slightly higher than k_BT at room temperature, this local minimum is unlikely to trap the molecule for any substantial period of time.

B. Excited-State Surfaces. The above molecular design assumed the simple cosine form of eq 3 for the excitation energy. Figure 9 shows results obtained for the vertical excitation energy of unsubstituted tolane as a function of dihedral angle generated using the INDO Hamiltonian and a direct single configuration interaction (SCI) method that includes excitations between all filled and empty molecular orbitals.[37] The ground-state geometry was optimized using SAM1, with a constraint applied only to the dihedral angle C1−C2−C5−C6.

The excited-state structure is considerably more complex than that of eq 3, with apparently strong mixing between excited states. A low-lying dark state is also predicted for all torsional angles. Spectroscopic measurements do find a low-lying dark state in tolane, but this dark state lies below the bright state only when the bridge between the phenyl rings bends,[34] whereas Figure 9 is for a linear bridge. The low-lying dark state is therefore attributed to an artifact from INDO theory. Although this bending about the bridge occurs in the excited state of bare tolane, the large steric groups present on the rings of the motor candidates will likely prevent such bending, so for the remainder of this analysis, we use the geometry obtained from optimizing the ground electronic state, in which the bridge remains nearly linear.

For tolane, the excited-state structure from INDO theory is considerably more complex then the simple form of eq 3. The form of eq 3 was derived by fitting the INDO excitation energy of PPE oligomers with three, four, and five rings. For these longer oligomers, delocalization lowers the excitation energy such that mixing between the lowest optically allowed states and higher states is reduced. For instance, such interactions are strong for the three-ring oligomer only when the molecule is highly twisted.[29] In addition, INDO only misidentifies the lowest state to be a dark state for tolane, and not for PPE oligomers with N larger than 2. Despite this artifact, we will next examine the excited-state energy surface of the bright state using INDO theory, before presenting results from ab initio theory.

Figure 7 shows the ground- and excited-state torsional surfaces for the best candidate motor, obtained using eq 3 (empty circles) with SAM1 for the ground-state energy and INDO for the excitation energy (filled symbols). We will consider the situation where the molecule is excited to the lowest bright state, i.e., the second excited state, S_2, in Figure 7. From the ground-state minimum, the oscillator strength to this second excited state is 25% of the oscillator strength at 0°, which is strongly optically allowed. The torsional potential in the bright state (S_2) is quite flat, but the global minimum is near 0°, and relaxation from this minimum is to a location on the ground-state surface that will lead to rotation in a CW direction. Using the ab initio result of Figure 8 for the ground-state energy, while retaining INDO for the excitation energy, leads to surfaces that are similar to those of Figure 7.

Figure 10 shows the torsional surfaces obtained using ab initio theory for both the ground-state and excitation energies. The geometries as a function of torsional angle are from the HF/3-21G calculations of Figure 8, with a constraint applied to only one dihedral angle (C1−C2−C5−C6). The ground-state energy in Figure 10 is obtained from single-point DFT calculations with the B3LYP density functional and a 6-31G(d,p) basis set. The excitation energy is from single-point TDDFT calculations, also using B3LYP/6-31G(d,p) theory. The ground-state surface shows a minimum at −70° that will contain most of the population at room temperature. Excitation is to a point on the excited-state surface that will relax in the CW direction. There is a local minimum at −30° and a global minimum at 20°, but these are fairly close in energy. Assuming the populations of these two minima are equal, on return to the ground state, half the population would rotate CCW back to the ground-state minimum at −70° and half the population would rotate CW to a new ground-state minimum at 110°. Therefore, half the population returns to the initial configuration upon optical excitation and subsequent relaxation, and half the population undergoes a 180° CW rotation upon absorption of a photon and subsequent relaxation. There is therefore a substantial net rotation of molecules on each absorption/relaxation cycle. For the excited-state surface in Figure 10, the minimum at 20°

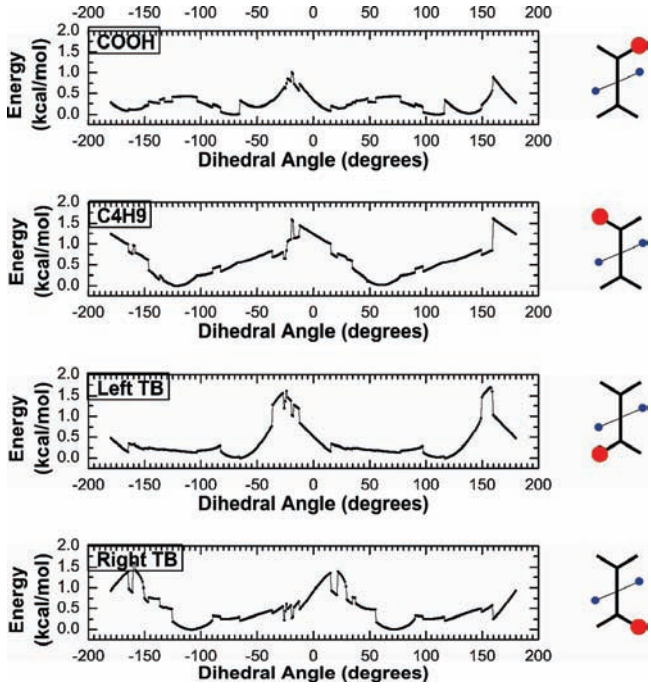

Figure 11. Decomposition of the SAM1 energy performed by replacing all but one steric group with hydrogen. "Left TB" refers to the isopropyl group on the lower portion of the rotor, and "Right TB" refers to the *tert*-butyl group on the lower portion of the rotor.

is 0.3 kcal/mol higher in energy than that at −30°, and an integration of the population densities suggests that the population ratio between the 20° minimum and −30° minimum is about 3/4. This will somewhat decrease the net rotation on excitation. Overall, although ab initio theory was not used to initially design the candidate motor, it supports the possibility of this molecule to undergo net rotation upon excitation. Note, however, that the computed excitation energy corresponds to vertical excitation. Full optimization of the excited-state structure was attempted but found to be computationally unfeasible with the available resources.

5. Decomposition of Energy

To better understand how the ground-state potential energy surface arises from the structural features of the molecule, we attempted to decompose the interactions between the rotor and each of the four substituents on the stator. This decomposition could be effected by generating the torsional surface for each of the four molecules shown schematically on the right of Figure 11, in which all but one group on the stator has been replaced with a hydrogen atom. Simply generating the torsional surfaces of each of these four molecules is not sufficient, however, due to the flexible nature of the molecule. In the full motor molecule, the structure distorts due to simultaneous interactions of the rotor with all four groups on the stator. These distortions differ considerably from those induced when only a single group is present on the stator. By constraining the geometry of the molecule to remain that present in the full molecule, we can better decompose the energy into the interactions present in the full molecule. This is done by replacing three of the four groups on the stator with hydrogen and calculating the energy with the geometry of the molecule constrained to that obtained in the full molecule, optimizing only the coordinates of the three hydrogen atoms added to the stator to replace the removed groups.

The results of the above computations are shown on the left of Figure 11. The structure of the full motor was first optimized

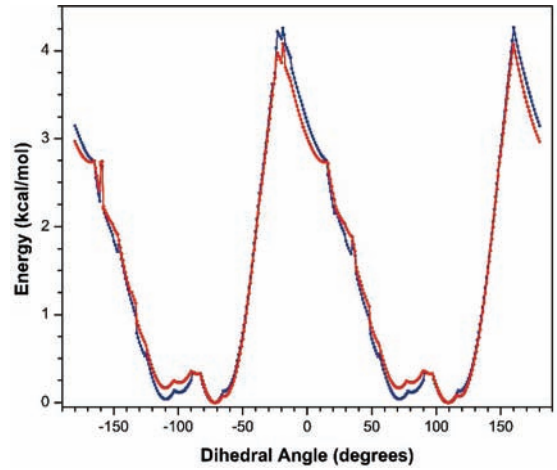

Figure 12. Sum of the decomposed interactions of the energy surface (blue) vs the energy surface of the full molecular motor (red).

with a single dihedral angle constraint (C1−C2−C5−C6) ranging from −180° to +180° in steps of +1°. At each new angle, the geometry optimization used, as a starting point, the geometry from the previous calculation. This led to the molecule finding local minima in some situations, as groups were slowly forced past one another until they snapped past one another and into a global minimum. To compensate for this, a sweep in the opposite direction was also performed, from +180° to −180° in steps of −1°. At each angle, the structure with the lowest energy was retained. This is the origin of the discontinuities in the individual interaction energies of Figure 11. These discontinuities are compensating and lead to a smooth energy surface when summed to give the total molecular energy, discussed next.

The degree to which the decomposition reflects the actual molecule was obtained by comparing the surface obtained by summing the decomposed energies to that of the full motor molecule. To allow for this summation, the energy of the framework was obtained by computing the energy with all four groups on the stator replaced with hydrogen. The energies of Figure 11 reflect the energy of the framework plus the interactions of the rotor with each group on the stator. To sum these to the total energy, we add the four energies of Figure 11 and then subtract 3 × the framework energy (since the summation contains the framework energy four times). The summed surface of Figure 12 is in good agreement with that of the full molecule and reproduces the key features discussed above that lead to unidirectional motion.

The agreement in Figure 12 suggests that the decomposition can be used to understand how these key features of the torsional surface arise from the interactions between the rotor and the four groups on the stator. One such key feature is the occurrence of the global minimum beyond 90°. This feature is present only in the molecules that contain the COOH and the Left TB substituents, implying this feature results from an attractive interaction between the rotor and these two groups. The other key feature is the occurrence of the maximum in the torsional surface at angles below 0°. This feature is present in all molecules except Right TB, implying that repulsive interactions with all groups except the Right TB contribute to this feature.

6. Conclusions and Future Work

The above results suggest that it may be possible to design a molecular motor on the basis of the tendency of a conjugated system to planarize in the excited state. The candidate motor molecule was designed using semiempirical quantum chemical

methods. Although the surfaces obtained using ab initio theory differ from those obtained using semiempirical theory, the ab initio surfaces also support the ability of the molecule to serve as a light-driven molecular motor. All of these surfaces were obtained by optimizing the ground-state geometry and so reflect vertical excitation energies. Full geometry optimization would help to better evaluate the ability of this molecule to serve as a motor and is left to future work.

The calculations performed here also ignore the solvent interactions. Those features of the potential energy surface that result from steric interactions between the rotor and stator will likely not be strongly altered by solvent interactions. However, one important feature, the location of the ground-state minimum, arises from an attractive interaction between the rotor and a polar group on the stator. This interaction has the disadvantage that it may be altered by solvent interactions. In addition, the use of a carboxylic acid group may be problematic, since this group can lead to pH sensitivity and specific interactions with hydrogen-bonding solvents. Replacing the carboxylic acid group with halogens was explored, but found not to retain the features required for molecular rotation.

In addition, we note that the computed excited-state structure of tolane is fairly complex and exhibits strong couplings between different excited states. The ability of the theory to model such interactions is not well tested here. These interactions also substantially lower the driving forces present in the excited state. The desired rotation on the ground-state surface (from 20° to 110° in Figure 10) has a strong driving force. However, the rotation from +110°/−70° to +20° on the excited-state surface is not strongly driven. This loss of driving force results from a flattening of the excited-state torsional potential, relative to that from the idealized excitation energy of eq 3, due to couplings between excited states (Figure 9). The couplings between different excited states may be considerably weaker in longer PPE oligomers,[29] since the increased conjugation lowers the energy of the optically active excited state relative to higher lying states. A motor based on a longer oligomer may therefore lead to stronger driving forces in the excited states.

Considerable additional work is needed to optimize these molecules and experimentally measure their motor characteristics. The potential advantage of this new class of molecular motors is that each of the processes required for a full rotation is expected to occur on the nanosecond time scale. Motors based on isomerizations often require a much slower thermal relaxation step. While an overall advantage in terms of use, this fast time scale may make experimental verification of the process more challenging, since trapping of intermediates along the rotational process will likely not be feasible. Design of experiments to measure and characterize unidirectional rotation remains a challenge.

Acknowledgment. The work was supported by the National Science Foundation (Grant CHE-0719350).

References and Notes

(1) Eelkema, R.; Pollard, M. M.; Vicario, J.; Katsonis, N.; Ramon, B. S.; Bastiaansen, C. W. M.; Broer, D. J.; Feringa, B. L. *Nature (London, U.K.)* **2006**, *440*, 163–163.

(2) Kelly, T. R.; Silva, R. A.; De Silva, H.; Jasmin, S.; Zhao, Y. *J. Am. Chem. Soc.* **2000**, *122*, 6935–6949.

(3) Koumura, N.; Zijistra, R. W. J.; Van Delden, R. A.; Harada, N.; Feringa, B. L. *Nature (London)* **1999**, *401*, 152–155.

(4) Joachim, C.; Gimzewski, J. K. *Struct. Bonding (Berlin, Germany)* **2001**, *99*, 1–18.

(5) Kelly, T. R.; De Silva, H.; Silva, R. A. *Nature (London)* **1999**, *401*, 150–152.

(6) Kelly, T. R.; De Silva, H.; Silva, R. A. *Acc. Chem. Res.* **2001**, *34*, 514–522.

(7) Dahl, B. J.; Branchaud, B. P. *Tetrahedron Lett.* **2004**, *45*, 9599–9602.

(8) Raehm, L.; Sauvage, J.-P. *Struct. Bonding (Berlin, Germany)* **2001**, *99*, 55–78.

(9) Hernandez, J. V.; Kay, E. R.; Leigh, D. A. *Science (Washington, DC, U.S.)* **2004**, *306*, 1532–1537.

(10) Hawthorne, M. F.; Zink, J. I.; Skelton, J. M.; Bayer, M. J.; Liu, C.; Livshits, E.; Baer, R.; Neuhauser, D. *Science (Washington, DC, U.S.)* **2004**, *303*, 1849–1851.

(11) Lin, Y.; Dahl, B. J.; Branchaud, B. P. *Tetrahedron Lett.* **2005**, *46*, 8359–8362.

(12) van Delden, R. A.; ter Wiel, M. K. J.; Pollard, M. M.; Vicario, J.; Koumura, N.; Feringa, B. L. *Nature (London, U.K.)* **2005**, *437*, 1337–1340.

(13) Fujita, T.; Kuwahara, S.; Harada, N. *Eur. J. Org. Chem.* **2005**, 4533–4543.

(14) Vicario, J.; Walko, M.; Meetsma, A.; Feringa, B. L. *J. Am. Chem. Soc.* **2006**, *128*, 5127–5135.

(15) Wang, L.; Hampel, F.; Gladysz, J. A. *Angew. Chem., Int. Ed.* **2006**, *45*, 4372–4375.

(16) Khuong, T.-A. V.; Nunez, J. E.; Godinez, C. E.; Garcia-Garibay, M. A. *Acc. Chem. Res.* **2006**, *39*, 413–422.

(17) Schoevaars, A. M.; Kruizinga, W.; Zijlstra, R. W. J.; Veldman, N.; Spek, A. L.; Feringa, B. L. *J. Org. Chem.* **1997**, *62*, 4943–4948.

(18) Leigh, D. A.; Wong, J. K. Y.; Dehez, F.; Zerbetto, F. *Nature (London, U.K.)* **2003**, *424*, 174–179.

(19) Magnera, T. F.; Michl, J. *Top. Curr. Chem.* **2005**, *262*, 63–97.

(20) Iwamura, H.; Mislow, K. *Acc. Chem. Res.* **1988**, *21*, 175–182.

(21) Kelly, T. R.; Bowyer, M. C.; Bhaskar, K. V.; Bebbington, D.; Garcia, A.; Lang, F.; Kim, M. H.; Jette, M. P. *J. Am. Chem. Soc.* **1994**, *116*, 3657–3658.

(22) Huck, N. P. M.; Jager, W. F.; de Lange, B.; Feringa, B. L. *Science* **1996**, *273*, 1686–1688.

(23) Ashton, P. R.; Ballardini, R.; Balzani, V.; Baxter, I.; Credi, A.; Fyfe, M. C. T.; Gandolfi, M. T.; Gmez-Lpez, M.; Martnez-Daz, M.-V.; Piersanti, A.; Spencer, N.; Stoddart, J. F.; Venturi, M.; White, A. J. P.; Williams, D. J. *J. Am. Chem. Soc.* **1998**, *120*, 11932–11942.

(24) Bissell, S. A.; Córdova, E.; Kaifer, A. E.; Stoddard, J. F. *Nature* **1994**, *369*, 133–136.

(25) Bedard, T. C.; Moore, J. S. *J. Am. Chem. Soc.* **1995**, *117*, 10662–10671.

(26) Kelly, T. R.; Sestelo, J. P.; Tellitu, I. *J. Org. Chem.* **1998**, *63*, 3655–3665.

(27) Okuyama, K.; Hasegawa, T.; Ito, M.; Mikami, N. *J. Phys. Chem.* **1984**, *88*, 1711–1716.

(28) Greaves, S. T.; Flynn, E. L.; Futcher, E. L.; Wrede, E.; Lydon, D. P.; Low, P. J.; Rutter, S. R.; Beeby, A. *J. Phys. Chem. A* **2006**, *110*, 2114–2121.

(29) Lu, L. T.; Yaron, D. J.; Sluch, M. I.; Berg, M. A. *J. Phys. Chem B* **2006**, *110*, 18844–18852.

(30) Lu, L. T.; Yaron, D. J.; Berg, M. A. *J. Phys. Chem. C* **2007**, *111*, 5770–5782.

(31) Hoki, K.; Sato, M.; Yamaki, M.; Sahnoun, R.; González, L.; Koseki, S.; Fujimura, Y. *J. Phys. Chem B* **2004**, *108*, 4916–4921.

(32) Larsen, D. S.; Ohta, K.; Fleming, G. R. *J. Chem. Phys.* **1999**, *111*, 8970–8979.

(33) Reynolds, L.; Gardecki, J. A.; Frankland, S. J. V.; Horng, M. L.; Maroncelli, M. *J. Phys. Chem.* **1996**, *100*, 10337–10354.

(34) Zgierski, M. Z.; Lim, E. C. *Chem. Phys. Lett.* **2004**, *387*, 352–355.

(35) AMPAC 8: Semichem, Inc., P.O. Box 1649, Shawnee, KS 66222, 1992−2004.

(36) Gaussian 03, revision C.02: Frisch, M. J.; Trucks, G. W.; Schlegel, H. B.; Scuseria, G. E.; Robb, M. A.; Cheeseman, J. R.; Montgomery, J. A., Jr.; Vreven, T.; Kudin, K. N.; Burant, J. C.; Millam, J. M.; Iyengar, S. S.; Tomasi, J.; Barone, V.; Mennucci, B.; Cossi, M.; Scalmani, G.; Rega, N.; Petersson, G. A.; Nakatsuji, H.; Hada, M.; Ehara, M.; Toyota, K.; Fukuda, R.; Hasegawa, J.; Ishida, M.; Nakajima, T.; Honda, Y.; Kitao, O.; Nakai, H.; Klene, M.; Li, X.; Knox, J. E.; Hratchian, H. P.; Cross, J. B.; Bakken, V.; Adamo, C.; Jaramillo, J.; Gomperts, R.; Stratmann, R. E.; Yazyev, O.; Austin, A. J.; Cammi, R.; Pomelli, C.; Ochterski, J. W.; Ayala, P. Y.; Morokuma, K.; Voth, G. A.; Salvador, P.; Dannenberg, J. J.; Zakrzewski, V. G.; Dapprich, S.; Daniels, A. D.; Strain, M. C.; Farkas, O.; Malick, D. K.; Rabuck, A. D.; Raghavachari, K.; Foresman, J. B.; Ortiz, J. V.; Cui, Q.; Baboul, A. G.; Clifford, S.; Cioslowski, J.; Stefanov, B. B.; Liu, G.; Liashenko, A.; Piskorz, P.; Komaromi, I.; Martin, R. L.; Fox, D. J.; Keith, T.; Al.Laham, M. A.; Peng, C. Y.; Nanayakkara, A.; Challacombe, M.; Gill, P. M. W.; Johnson, B.; Chen, W.; Wong, M. W.; Gonzalez, C.; Pople, J. A. Gaussian, Inc., Wallingford, CT, 2004.

(37) Tomlinson, A.; Yaron, D. *J. Comput. Chem.* **2003**, *24*, 1782–1788.

JP811521S